The virtual node polygonal element method for fatigue crack growth simulation

***Z.H. Teng[1], † D.M. Liao[1], S.C. Wu[2], Z. B. Zhang[1], T. Chen[1], F. Sun[1]**

[1] State Key Lab. of Material Processing and Die & Mould Technology, Huazhong University of Science & Technology, China

[2] State Key Lab. of Traction Power, Southwest Jiaotong University, China

*Presenting author: tengzihao@hust.edu.cn

†Corresponding author: liaodunming@hust.edu.cn

Abstract

Simulation of fatigue crack propagation and prediction of structural life is crucial to ensure the safety of engineering structure. The standard Extended Finite Element Method (XFEM) requires sufficiently fine mesh for crack propagation problems, which is computationally expensive and inconvenient to operate. In the present work, a simple dynamic adaptive mesh refinement method is proposed using the Virtual-node Polygonal Element method within the framework of the XFEM. Through this method, a multi-level refinement of the custom region near the crack tip can be realized. The refinement area changes dynamically with the crack tip position during the crack propagation process, so that the demands of the computational cost and accuracy can be reconciled. The domain based interaction integral approach is used to obtain the stress intensity factors(SIFs). The propagation direction of the crack is determined by the maximum circumferential stress criterion and the fatigue life of the cracked structure is evaluated by Paris Law. Then two simple examples are presented and the accuracy and convergence of the algorithm are verified. Compared with the standard XFEM, the proposed method requires far fewer degrees of freedom for the same accuracy. Finally, two fatigue crack growth problems are solved, and the SIFs and fatigue life cycle show good agreement with the results available in literature.

Keywords: Polygonal element method, Dynamic adaptive mesh refinement, Fatigue crack growth

Introduction

Many engineering structures will bear the effect of cyclic load during the service process. It is very important to study the propagation behavior of the crack under cyclic loading to ensure the safety of the structure. The study of fatigue crack propagation path and the prediction of structure life cycle has being a research focus in recent years. Over the last few decades, the Finite Element Method has been widely used in the analysis of fracture problems, and a lot of commercial software and open source software packages have emerged. Due to the fact that the mesh must be aligned with the crack surfaces in FEM, re-meshing is needed once the crack is propagated, which limits the application of FEM in dynamic crack propagation simulation. In order to solve this problem, researchers have proposed many new methods, such as meshless

method[1]-[4], boundary element method (BEM)[5][6], superposition FEM[7][8], and extended finite element method (XFEM)[9]-[13]. Among these algorithms, XFEM has gained the most attentions for dynamic fracture problems with the discontinuities[14]-[16]. The key point is that augmented XFEM space of alive cracks is achieved by adopting the enrichment functions in terms of partition of unity (PU) and mesh is not required to be aligned with the crack surfaces.

Although XFEM can achieve better results in simulations of fatigue crack propagation, it is difficult for XFEM to balance the computational accuracy and computational efficiency for large and complex structures[17]. To ensure the accuracy of the stress intensity factors(SIFs) near the crack tip, it is necessary to set a fine mesh around the crack tip. On the other hand, to accurately characterize the actual crack propagation path, the crack growth increment should not be too large at each step, which also requires that the mesh near the crack tip should not be too coarse[16]. However, the location of crack tips are changing since the crack is propagated, a fine mesh for the whole domain or a local mesh refine method is needed to tackle the above problem. A fine global mesh will greatly decrease the computational efficiency while local mesh refine always needs to bring in transition elements and it will face the problem of mesh coarsening when the position of crack tips changes.

To solve the problems mentioned above, a multi-level adaptively refined mesh in XFEM at the crack tip is formulated by introducing virtual node polygonal element method (VPM) for solving elastic fracture mechanics. The foremost merit of proposed dynamic mesh refinement strategy is that the refine domain can be automatically moved with the crack tip without transition elements. Moreover, this method only needs to modify the shape function of the element and can be easily added to the existing XFEM program framework. This method has been applied to transient temperature field soldering in laser welding[19] and thermal fatigue crack propagation prediction[17].

Brief on the VP-XFEM

Small-deformation based homogeneous isotropic and linear-elastic cracked domain is considered here to derive the partial differential equations with VP-XFEM.

Governing equations

A 2D homogenous problem domain Ω without considering any discontinuities can be discretized into *N* polygonal elements with arbitrary nodes in VP-XFEM. The boundary Γ can be partitioned into the displacement Γ_u, the traction Γ_t and the traction free Γ_c. Thus the equilibrium conditions and boundary conditions are given as

$$\nabla \cdot \boldsymbol{\sigma} + \mathbf{b} = 0 \quad \text{in } \Omega \tag{1}$$

$$\mathbf{u} = \mathbf{u}_\Gamma \quad \text{at } \Gamma_u \tag{2}$$

$$\boldsymbol{\sigma} \cdot \mathbf{n} = \mathbf{t}_\Gamma \text{ at } \Gamma_t \tag{3}$$

$$\boldsymbol{\sigma} \cdot \mathbf{n} = 0 \quad \text{at } \Gamma_c \tag{4}$$

where ∇ is the divergence operator, $\boldsymbol{\sigma}$ is the Cauchy stress tensor and $\mathbf{b}$ is the body force term, $\mathbf{u}_\Gamma$ and $\mathbf{t}_\Gamma$ are the vectors of the prescribed displacements and tractions, respectively. The unit vector $\mathbf{n}$ is defined as the outward normal to the boundary Γ.
The constitution relationship is given by

$$\boldsymbol{\sigma} = \mathbf{D}\boldsymbol{\varepsilon} \tag{5}$$

$$\boldsymbol{\varepsilon} = \left[\nabla\mathbf{u} + \left(\nabla\mathbf{u}\right)^{\mathrm{T}}\right]/2 \tag{6}$$

where $\mathbf{D}$ is the matrix of material constants and $\boldsymbol{\sigma}^{\mathrm{T}}=\{\sigma_{xx}, \sigma_{yy}, \sigma_{xy}\}$ and $\boldsymbol{\varepsilon}^{\mathrm{T}}=\{\varepsilon_{xx}, \varepsilon_{yy}, \varepsilon_{xy}\}$ are the vectors of the stress and strain tensor, respectively. $\mathbf{u}=\{u, v\}^{\mathrm{T}}$ is the vector of the assumed displacement with newly-developed VP-XFEM.

VPM shape function

Assuming that a problem domain Ω bounded by Γ is discretized by N polygonal elements. For a given n-nodes polygon that can be divided into n virtual sub-triangles, the shape function of VPM consists of two components: the least-squares method (LSM) and the constant strain triangular element (CST). Assuming a point of interest p_l with the Cartesian coordinates $\mathbf{x}^{\mathrm{T}}=$(x, y, z), the shape function in VPM can be defined as

$$\Phi_l\left(\mathbf{x}\right) = W_{\mathrm{I},i}\left(\mathbf{x}\right)\left[\left(\delta_{il}+\delta_{jl}\right)\varphi_l\left(\mathbf{x}\right)+\varphi_k\left(\mathbf{x}\right)\psi_l\left(\mathbf{x}\right)\right]+W_{\mathrm{II},i}\left(\mathbf{x}\right)\psi_l\left(\mathbf{x}\right) \tag{7}$$

where the subscript i of weight function W_{I} from CST and weight function W_{II} from LSM represents that the point p_l is located inside the given sub-triangle T_i, the subscript k stands for the k-th polygonal element in the discretized domain. Note that weight functions W_{I} and W_{II} are assigned as $W_{\mathrm{I}}=\varphi_i+\varphi_j$ and $W_{\mathrm{I}}=-\varphi_k$ in which the subscript i, j and k represent the local nodal number of a sub-triangle. φ and ψ are shape functions based on the area or volume coordinates of CST and LSM, respectively.

VP-XFEM approximations

The displacement vector $\mathbf{u}_{\mathrm{XFEM}}$ in a cracked domain is

$$\mathbf{u}_{\mathrm{XFEM}}\left(\mathbf{x}\right) = \sum_{i\in I}\mathbf{u}_i\phi_i\left(\mathbf{x}\right)+\sum_{j\in J}\phi_j\left(\mathbf{x}\right)H\left(\mathbf{x}\right)\mathbf{a}_j+\sum_{k\in K}\phi_k\left(\mathbf{x}\right)\sum_{\alpha=1}^{4}\chi_\alpha\left(\mathbf{x}\right)\mathbf{b}_{k\alpha} \tag{8}$$

where I, J and K are the number of all nodes, that of interested nodes of bisected support and that of enriched nodes of bounded crack tip support, respectively; $\mathbf{u}_i$ and ϕ_i or ϕ_j are the displacement vector and shape function associated with node i or j of standard FEM, respectively; $\mathbf{a}_j$ are the additional degree of freedoms (DOFs) of bisected support by a crack path, $\mathbf{b}_k$ are the enriched DOFs associated with node k of crack tip region. $H(\mathbf{x})$ is the Heaviside function and χ_α is the component of crack tip enrichment function $\psi_\alpha(\mathbf{x})$ in which α=1, 2, 3, 4 as below

$$H\left(\mathbf{x}\right)=1 \text{ if } \left(\mathbf{x}-\mathbf{x}'\right)\cdot\mathbf{n}\geq 0;\ \text{otherwise } H\left(\mathbf{x}\right)=-1 \tag{9}$$

$$\psi_\alpha\left(r,\theta\right)=\left\{\sqrt{r}\sin\frac{\theta}{2},\quad \sqrt{r}\cos\frac{\theta}{2},\quad \sqrt{r}\sin\frac{\theta}{2}\sin\theta,\quad \sqrt{r}\cos\frac{\theta}{2}\sin\theta\right\} \tag{10}$$

where r and θ are the polar coordinates of interested point $\mathbf{x}$ with its origin crack tip.

Since the equation (8) is inconvenient for the imposing of essential displacement boundary conditions, the displacement requires to be further modified by replacing the enrichment functions with VP-XFEM as[14]

$$\mathbf{u}_{\text{VP-XFEM}}(\mathbf{x}) = \sum_{i\in I}\mathbf{u}_i\phi_i(\mathbf{x}) + \sum_{j\in J}\phi_j(\mathbf{x})\left[H(\mathbf{x}) - H(\mathbf{x}_j)\right]\mathbf{a}_j + \sum_{k\in K}\phi_k(\mathbf{x})\sum_{\alpha=1}^{4}\left[\chi_\alpha(\mathbf{x}) - \chi_\alpha(\mathbf{x}_k)\right]\mathbf{b}_{k\alpha} \tag{11}$$

Dynamic adaptive mesh refinement

VP Shape function continuity

Taking the quadrilateral for an exemplified data structure (see Fig. 1), the sub-quadrilateral element ① is further divided into four elements of ①, ⑤, ⑥ and ⑦. Thus the elements of ② and ③ have the hanging nodes of d and e, respectively. However in the VP-XFEM, there are no hanging node any more. All elements are recalled as polygonal element with variable *n* nodes, which can be treated by a VP shape function.

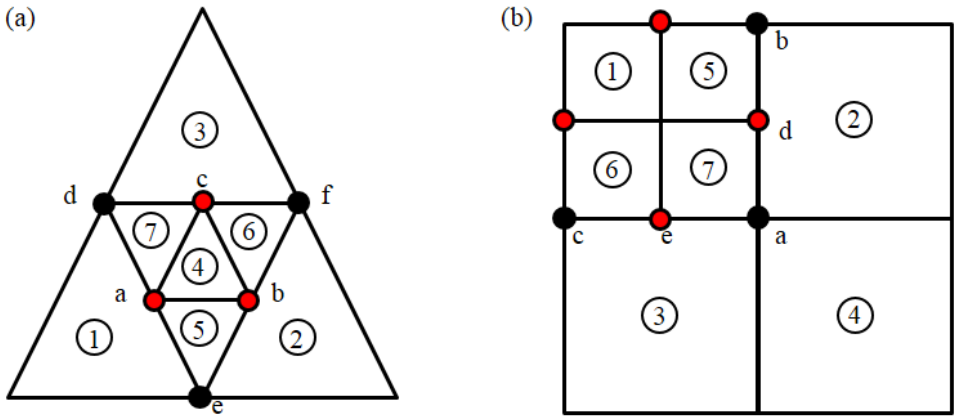

Fig. 1. The locally refined scheme with hanging nodes assigned as polygonal elements with variable *n* nodes: (a) the triangle based refinement; (b) the quadrilateral based refinement.

Based on the VP shape function in Eq. (7), the shape functions inside mixed or hybrid elements are depicted in Fig. 2. It is clearly observed that the VP shape functions possess a good continuity even near the hanging nodes. Such excellent property provides a feasible method to refine the mesh at the crack tip.

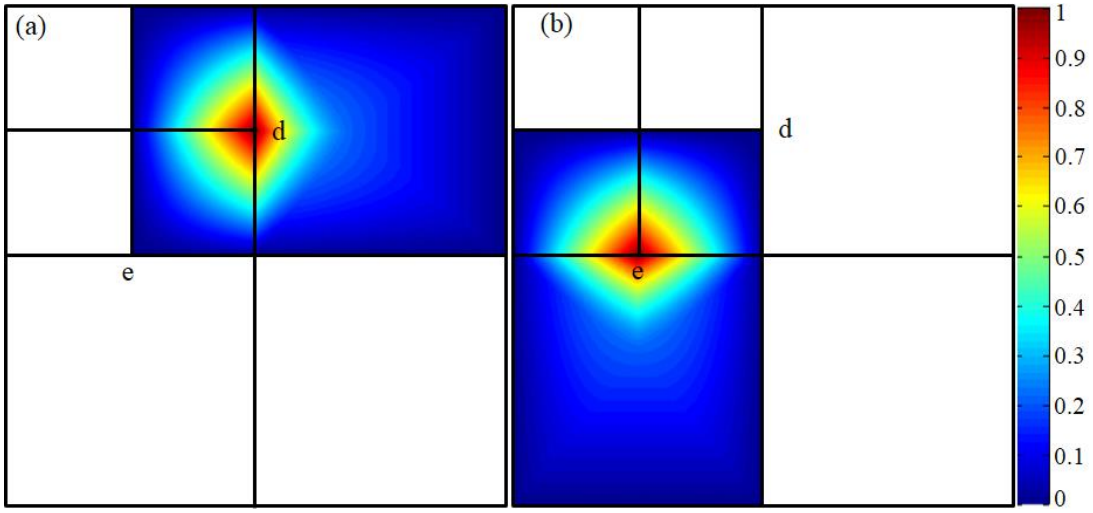

Fig. 2. The VP shape functions near hanging nodes of quadrilateral elements, in which the shape functions in (a) for d and (b) for e are zero over parts of the surrounding elements.

Single-step dynamic refinement

Based on linear elastic fracture mechanics, fatigue crack growth can be considered as a successive incident happened in the cyclic plastic zone ahead of a growing crack tip. An increment of crack extension is usually assumed to simulate the cracking process. To highlight the accuracy, a sing-step dynamic refinement algorithm is proposed along the crack path for an example of the four-point bending beam[17].Firstly, the refinement level L_r (≤ 4) and initial refinement dimension R_d are given in terms of $R_d=\alpha_r L_{max}$, in which α_r and L_{max} are the modeling parameter (α_r = 0.1~0.2 in view of the computational efficiency) and the maximum length of meshing box, respectively. Then the refinement radius of the i-th refinement level for a cracked problem can be taken as

$$r_i = R_d \beta^{i-1} \left(0 < \beta < 1\right) \tag{12}$$

where β is the refinement coefficient with an optimum value of 0.5.

For the nodes located in a circle with the radius r_i, all elements connected with those nodes require to be refined. Note that the identified circle is centered by the crack tip as shown in Fig. 3. However for multiple cracks in red herein, a domain union is created when multi cracks are available, as illustrated in Fig. 3.

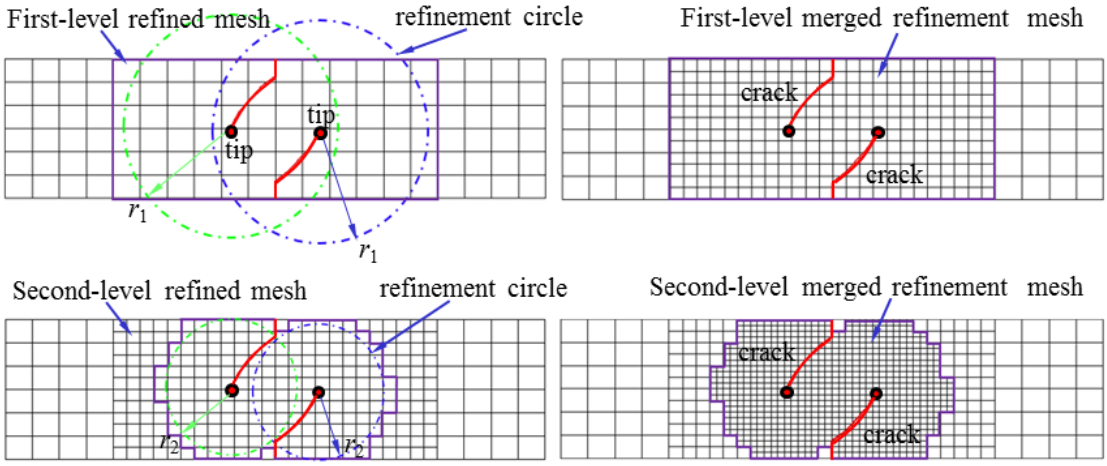

Fig. 3. The dynamic refinement of typical quadrilateral elements and the merged meshing regions around the crack after two meshing refinement operations.

Multi-step dynamic refinement

To achieve a good balance between accuracy and efficiency, two sets of meshing are introduced to deal with the refinement process. The initial background mesh with coarse elements (called the base mesh here) is stored by the first meshing set and keeps the same throughout the dynamic crack growth. The second meshing set is created dynamically with a growing crack tip, which is refined only at the crack tip with a single-step method. Fig. 4 presents the flowchart of the multi-step dynamic refinement around the crack tip with VP-XFEM.

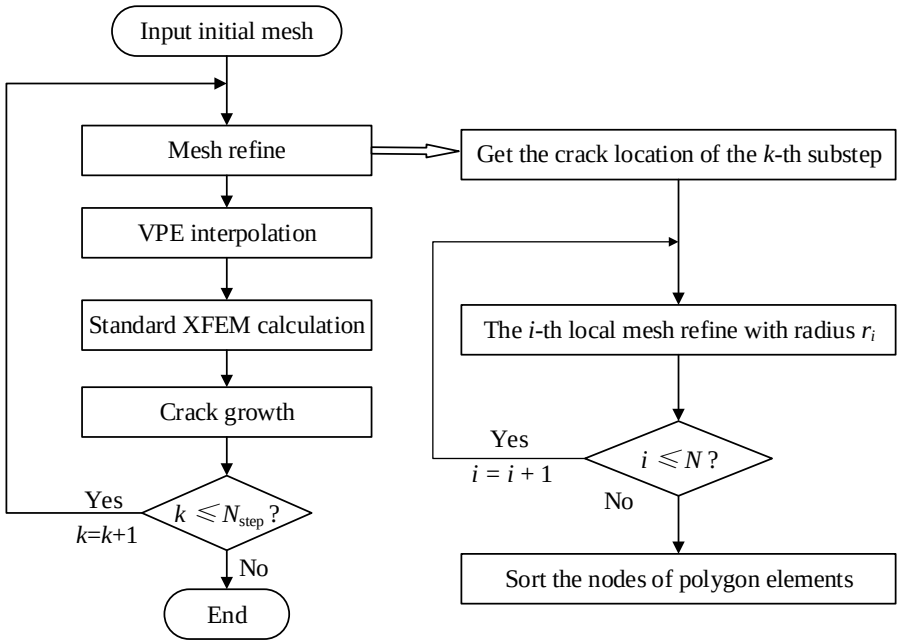

Fig. 4. A flowchart for the multi-step dynamic mesh refinement concept only around the crack tip during a typical fatigue crack growth simulation.

It is evidently seen from the flowchart that the initial background mesh is kept constant during the whole simulation and the local refinement from Eq. (12) is always conducted according to the position of a growing crack tip. The refined meshes on the crack path are retrieved to the

initial background mesh when the crack tip goes through the region. Here the four-point bending is used to present the concept as illustrated in Fig. 5. With the VP-XFEM in above Fig. 5, a four-level refined elemental meshing has been ideally realized with the movement of the crack tip for different incremental steps. The most significant advantage of current adaptively refined XFEM with the VP shape functions is actually independent of standard XFEM codes.

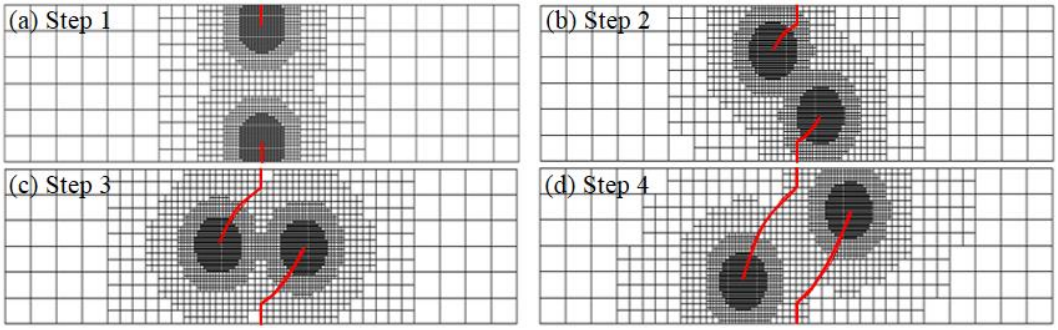

Fig. 5. The implementation of the dynamically local refinement meshing always at the crack tips with VP-XFEM, where the refined elements are bounded in terms of Eq. (12).

Crack growth modeling

For a 2D engineering crack under complex stress state, the domain based interaction integral approach is used to obtain the SIFs[10], and the maximum circumferential stress criterion is used to determine the dynamic crack growth direction

$$\theta_{\mathrm{c}} = 2\arctan\left(\frac{K_{\mathrm{I}} \pm \sqrt{K_{\mathrm{I}}^2 + 8K_{\mathrm{II}}^2}}{4K_{\mathrm{II}}}\right), \quad -\pi < \theta_{\mathrm{c}} < \pi \tag{13}$$

Under constant fatigue loading, the SIF range ΔK can be calculated by

$$\Delta K = K_{\max} - K_{\min} \tag{14}$$

where $K_{\max}$ and $K_{\min}$ are the maximum and minimum SIFs, respectively. The effective SIF range of ΔK_{eff} can thus be determined in terms of mode I cracking SIF range or ΔK_{I} and mode-II cracking SIF range or ΔK_{II} when approaching the critical angle θ_{c} by

$$\Delta K_{\mathrm{eff}} = \Delta K_{\mathrm{I}} \cos^3\left(\frac{\theta_{\mathrm{c}}}{2}\right) - 3\Delta K_{\mathrm{II}} \cos^2\left(\frac{\theta_{\mathrm{c}}}{2}\right)\sin\left(\frac{\theta_{\mathrm{c}}}{2}\right) \tag{15}$$

To predict the residual life of a cracked component based on elastic fracture mechanics, the proper selection of fatigue crack growth rate law is a fundamental issue for long cracks, and classical Paris model is probably the most useful in practice as

$$\frac{\mathrm{d}a}{\mathrm{d}N} = C\left(\Delta K_{\mathrm{eff}}\right)^m \tag{16}$$

where a and N are the crack extension and reversed cycles, respectively. C and m are the material parameters determined also dependent of testing conditions. Once crack growth resistance and crack driving force are known for a single standard crack, fatigue growth life can be integrated in terms of Eq. (16) under constant crack extension Δa. On the other hand, the

maximum crack extension $\Delta a_{\max}$ is assumed to be constant in case of an arbitrary-orientated crack or multi cracks. Therefore, the incremental length for any crack front point from VP-XFEM can be calculated by

$$\Delta a = \Delta a_{\max} \left(\frac{\Delta K_{\text{eff}}}{\Delta K_{\text{eff,max}}} \right)^{m} \tag{17}$$

where $\Delta K_{\text{eff,max}}$ is the maximum nodal ΔK_{eff} among all front points of a crack. It should be noted that the cracking simulation is stopped automatically when nodal $\Delta K_{\text{eff,max}}$ at a point of crack front is larger than measured fracture toughness K_{mat} of a material.

Numerical results

This sections verify the novel VP-XFEM models in terms of accuracy, convergence and efficiency by using different pre-cracked problems with or without analytical solutions. For quantitative examinations of the performance of proposed VP-XFEM in contrast with standard XFEM, two types of normalized error norms are introduced including the displacement error norm E_{u} and the energy error norm E_{e} as

$$E_{\text{u}} = \left\| \mathbf{u}^{\text{exa}} - \mathbf{u}^{\text{app}} \right\|_{L_2(\Omega)} = \sqrt{\frac{\int_{\Omega} \left(\mathbf{u}^{\text{exa}} - \mathbf{u}^{\text{app}} \right)^{\text{T}} \left(\mathbf{u}^{\text{exa}} - \mathbf{u}^{\text{app}} \right) \text{d}\Omega}{\int_{\Omega} \left(\mathbf{u}^{\text{exa}} \right)^{\text{T}} \left(\mathbf{u}^{\text{exa}} \right) \text{d}\Omega}} \tag{18}$$

$$E_{\text{e}} = \left\| \frac{\boldsymbol{\varepsilon}^{\text{exa}} - \boldsymbol{\varepsilon}^{\text{app}}}{\boldsymbol{\varepsilon}^{\text{exa}}} \right\| = \sqrt{\frac{\int_{\Omega} \left(\boldsymbol{\varepsilon}^{\text{exa}} - \boldsymbol{\varepsilon}^{\text{app}} \right)^{\text{T}} \text{D} \left(\boldsymbol{\varepsilon}^{\text{exa}} - \boldsymbol{\varepsilon}^{\text{app}} \right) \text{d}\Omega}{\int_{\Omega} \left(\boldsymbol{\varepsilon}^{\text{exa}} \right)^{\text{T}} \text{D} \left(\boldsymbol{\varepsilon}^{\text{exa}} \right) \text{d}\Omega}} \tag{19}$$

where the subscripts of u and e represent the displacement and energy norms, respectively. While the superscripts of exa and app stand for the approximate and exact or reference solutions to the displacement, strain and stress, respectively.

Linear patch test

The first example is to perform a patch test that is widely used in standard FEM. Three patches as shown in Fig. 6 are examined in terms of computational accuracy. Fig. 7 (a) gives a patch with 20 normal quadrilaterals, Fig. 8 (b) gives one with 26 polygonal elements where two rectangles are further divided into four quadrilaterals, thus producing 3 hanging nodes of each element. Finally, Fig. 9 (c) shows one with arbitrary-distributed and different-sized polygonal or mixed elements.

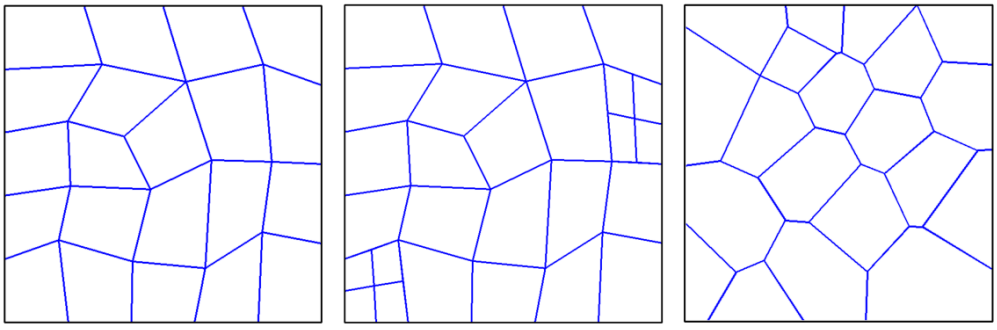

Fig. 10. Three typical meshes used for the patch tests: (a) perturbed quadrilateral mesh, (b) locally refined quadrilateral mesh and (c) full-field polygonal mesh.

The material parameters used in the testing are assumed as: Young's modulus of E=1.0 and Poisson's ratio of v=0.3. Note that in the work the international standard unit system is based unless specially denoted. For all patches, the displacements are prescribed along all boundaries by a linear basis of x and y as[20]

$$u = 1 + x + y \tag{20}$$

$$v = 1 - x + 2y \tag{21}$$

For a fully discontinuous domain or a problem without a crack, the XFEM is actually equivalent to standard FEM as built in Eq. (8). As a relatively fair comparison, 2×2 Gaussian integration scheme is employed for standard XFEM. While only one integration point into each virtual triangles adopted for VP-XFEM proposed. Table 1 lists the errors of different meshing schemes for both XFEM and novel VP-XFEM. It is found that newly-proposed VP-XFEM using local polygonal shape functions can pass the patch tests within machine precision, showing that current VP-XFEM can exactly reconstruct a linear function of imposed displacements.

Table 1. Relative errors for three mesh cases of standard finite elements, hybrid finite elements with hanging nodes and full-filed polygonal elements.

Error norms	Models	Mesh A	Mesh B	Mesh C
E_u	XFEM	3.50057e-14	—	—
	VP-XFEM	2.90270e-15	8.55441e-15	2.52088e-14
E_e	XFEM	1.11148e-14	—	—
	VP-XFEM	1.77698e-15	4.40240e-15	1.25195e-15

Besides, current VP-XFEM presents higher accuracy compared with standard XFEM. Furthermore, for locally refined elements with hanging nodes and irregularly polygonal elements, current VP-XFEM model with at least linear consistency can still satisfy the patch test at better accuracy. In contrast, original XFEM cannot cope with the problems with hanging nodes and polygonal elements.

Plate with an edge crack

The next problem is an edge-crack finite width plate of size 90mm×108mm under cyclic tensile load of F_{min}=8kN and F_{max}=16kN[16], the initial crack length a=45mm and the thickness of the plate is 6mm as shown in Fig. 7, some material parameters are taken as:Young modulus E=200GPa, Poisson's v=0.30, Paris exponent m=2.1, Paris constant C=7×10^{-8}.

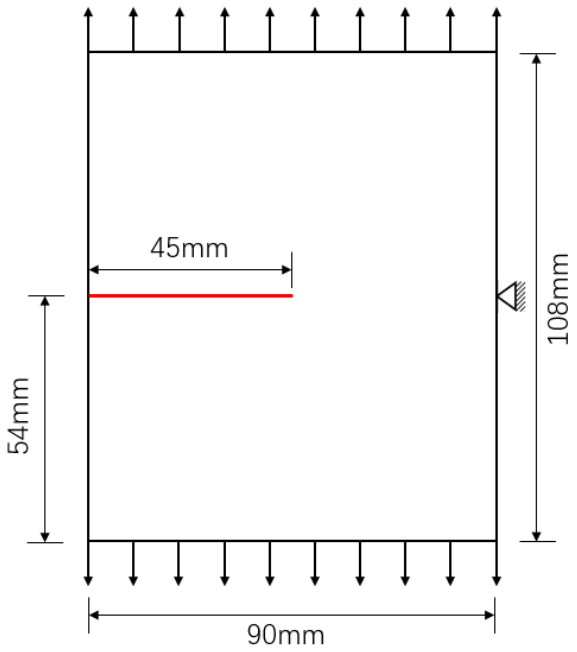

Fig. 11. Edge crack problem with a pre-crack subjected to cyclic tensile load.

The problem is solved by standard XFEM and VP-XFEM, the results are compared with the VNXFEM[16] and the experiment[21]. A uniform mesh of size 30×40 nodes is used with crack growth increment of 4.0mm for standard XFEM while the same mesh but with crack growth increments of 2.0mm and 4.0mm is used for VNXFEM. As for VP-XFEM, a coarse mesh of size 20×30 nodes is used and the refine radius α_r=0.15, refine level N=3 with crack growth increment of 2.0mm. Fig. 8 shows the variation of ΔK_{eff} as the crack grows. It can be seen that the three methods are all in good agreement with the experiment result. Besides, the VP-XFEM result is closer to the experiment through the partial amplification drawings. Moreover, the total DOFs of VP-XFEM is about 2500 to 2600 while the XFEM DOFs is around 2500, which demonstrates the computational efficiency of VP-XFEM. It is worth mentioning that the crack growth increment must be larger than the mesh size in standard XFEM, the VNXFEM breaks this limit by the partition of crack tip element, while the novel VP-XFEM achieves the same goal through the refinement of elements around the crack tip.

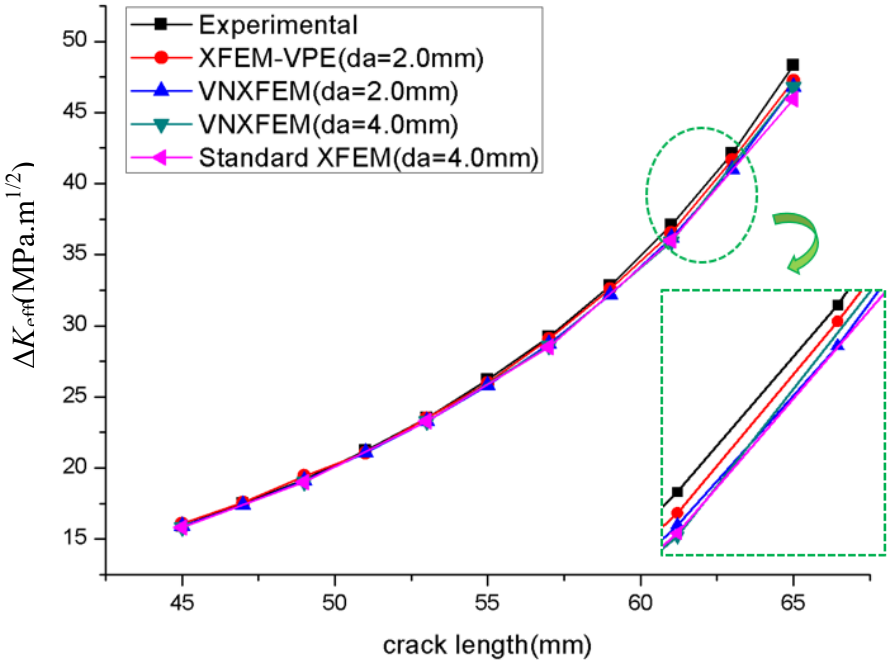

Fig. 12.The ΔK_{eff} variation with crack length of different cases.

Two internal non-colinear cracks

Based on newly-proposed VP-XFEM, this section performs a nonlinear analysis of fatigue crack growth of a rectangular plate ($90\times180\text{mm}^2$) subjected to reversed cyclic loading. In the middle of the plate under a cyclic tension ($\sigma_{\max}$=160MPa, $\sigma_{\min}$=0, then the stress ratio R=0, see Fig. 13) at both remote edges, there are two non-collinear and parallel straight cracks with the initial length a_0=10mm[4]. Moreover, the horizontal and vertical distances between two crack tip points (A) are 15mm and 5mm, respectively.

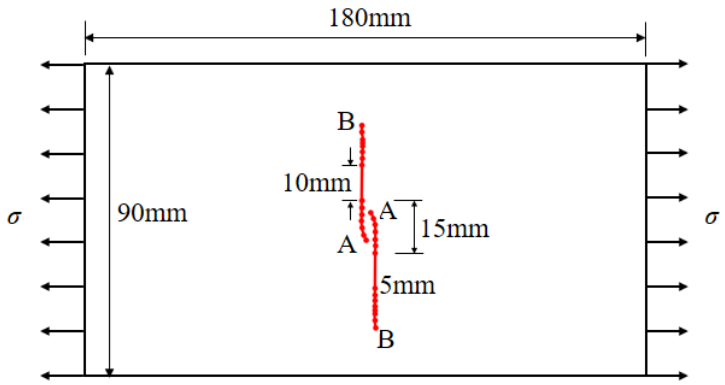

Fig. 13. Calculated cracking paths in a finite sized rectangular plate with two non-collinear cracks under cyclic tension loading at the stress ratio of R=0.

The material properties of fatigue resistance are taken as: E=74GPa, v=0.3, the fracture toughness of K_{mat}=1897.35N/mm$^{3/2}$, the Paris law based fatigue cracking parameters of C=2.087136×10^{-13} and m=3.32. The problem domain is discretized with nodes of 30×60 as an

initial background mesh for the VP-XFEM. In the fatigue cracking simulation, some parameters are taken as: the initial refinement radius is $0.1L_{max}$, the refinement level is L_r=4 and the crack increment is Δa_{max}=2mm. Note that for dynamic fracture mechanics, the large refinement level and high refinement radius should be adopted for better accurate SIFs solutions to determine the cracking direction and rate.

The evolutions of the SIF ranges ($\Delta K_{I,A}$, $\Delta K_{I,B}$, $\Delta K_{II,A}$ and $\Delta K_{II,B}$) and the effective SIF range ($\Delta K_{eff,A}$ and $\Delta K_{eff,B}$ in terms of Eq. (15)) at the most interior crack tips (A) and the crack tips near the edge (B) with the crack extension a_i is plotted in Fig. 14 and Fig. 15, respectively. As a comparison in this figure, numerical solutions from meshless method are available with totally 1416 nodes to discretize the same rectangular plate.

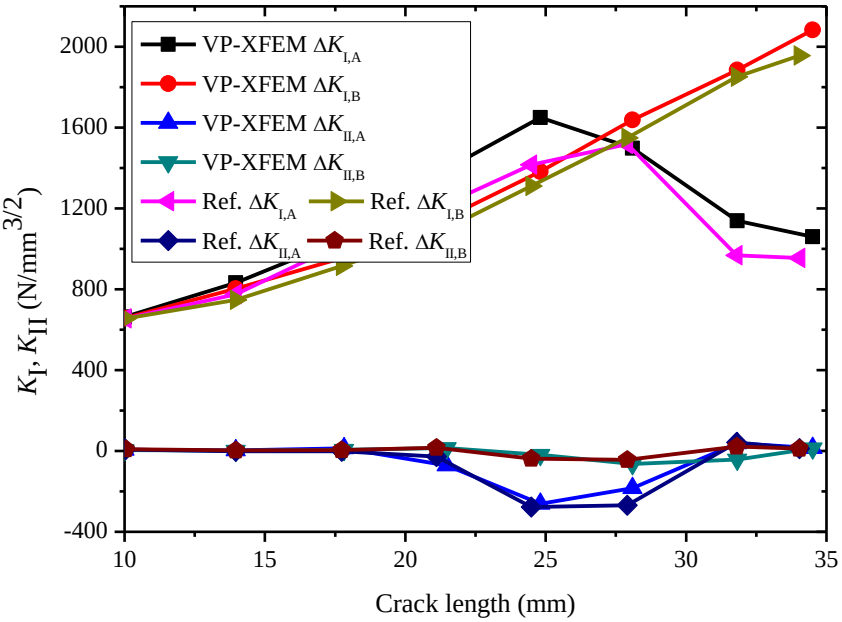

Fig. 14. The curves of SIF ranges of both points A and B with the crack length under a cyclic tension, in which meshless solutions are also provided for a comparison.

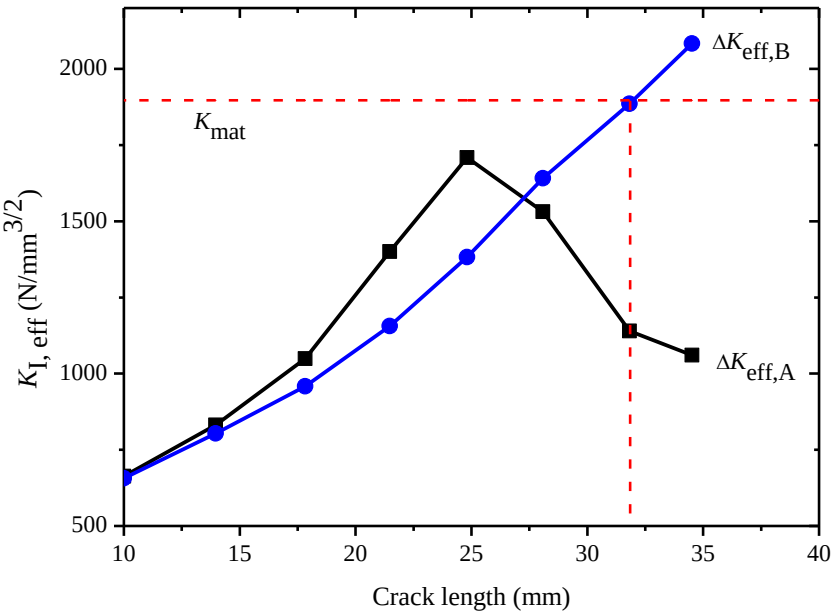

Fig. 15. The curves of effective SIF ranges of both points A and B with the crack length under a cyclic tension, in which the fracture toughness is provided to bound the cracking process.

Compared with meshless solutions with almost the DOFs, the present VP-XFEM always provides the larger SIF ranges at both points A and B, which shows an over-estimation results for a damaged body. At the starting of the cyclic loading, both $\Delta K_{II,A}$ and $\Delta K_{II,B}$ are basically zero to be a purely mode-I cracking problem. In contrast, the mode I fracture parameter $\Delta K_{I,A}$ of point A increases more rapidly than $\Delta K_{II,B}$ of point B until the mode II fracture parameter $\Delta K_{II,A}$ becomes negative. It is reasonably believed that the interaction due to crack tip stress fields happens with the crack extension of 25mm. However this phenomenon vanishes rapidly once the overlapping of two crack tips A takes place due to stress relaxation, showing a decreasing of the SIF ranges.

The effective SIF ranges in Fig. 15 are therefore feasible to evaluate the fatigue cracking process in terms of near-zero mode II fracture parameters. When the effective SIF range at point B exceeds the fracture toughness, an unstable fracture occurs. It is clearly seen that the predicted crack paths with lines in red are good agreement with both results of meshless method and experiments[4]. Based on the calculated SIF ranges of $\Delta K_{eff,A}$ and $\Delta K_{eff,B}$, the final fatigue crack growth life can be acquired in terms of Eq. , as illustrated in Fig. 16 for both points A and B together with total values. It is found that for the same crack extension, the VP-XFEM provides a short fatigue life. The residual life of the similar cracked component is predicted as 6630 cycles, which well coincides with the experiment.

(16)

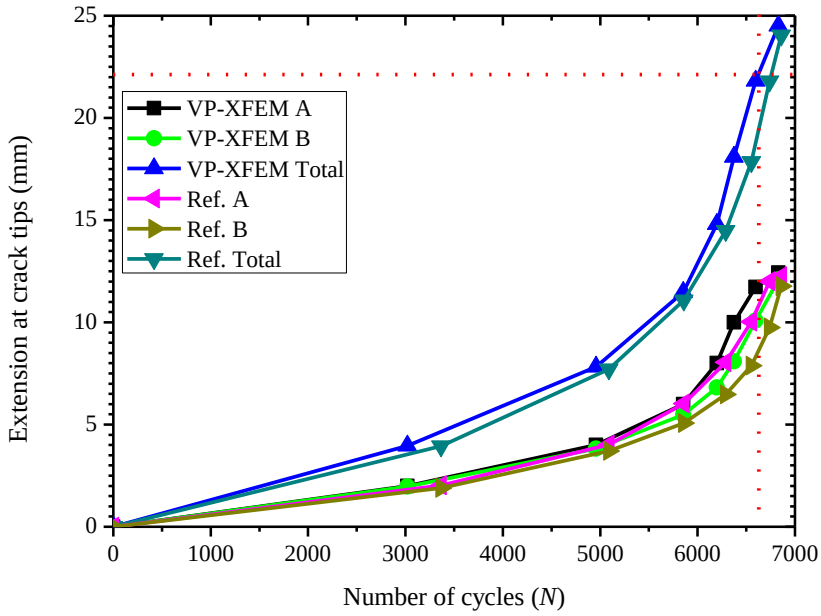

Fig. 16. Crack extension-Number of cyclic loading diagram.

Conclusions

In this paper, a theoretical study and an intensive numerical investigations on the newly-developed virtual polygonal elements based XFEM (VP-XFEM) have been carried out in terms of the local adaptive refinement strategy at the crack tip. The numerical results of VP-XFEM fully illustrate the advantages of the proposed method. The balance of computational accuracy and efficiency can be achieved by adjusting the refine parameters. Moreover, this method can be easily expanded to three dimensional problems.

References

[1] Belytschko T, Lu YY, Gu L. Element-free galerkin methods. Int J Numer Methods Eng 1994;37:229–256.

[2] Belytschko T, Lu YY, Gu L. Crack propagation by element-free Galerkin methods. Engrg.Fracture Mech 1995;51:295–315.

[3] Belytschko T, Krysl P. The Element Free Galerkin method for dynamic propagation of arbitrary 3-D cracks. Int J Numer Methods Eng 1999;44:767–800.

[4] Marc Duflot, Hung Nguyen-Dang. Fatigue crack growth analysis by an enriched meshless method. J Comput Appl Math 2004;168:155–164.

[5] Portela A, Aliabadi M, Rooke D. The dual boundary element method: effective implementation for crack problem. Int J Numer Methods Eng 1991;33:1269–1287.

[6] Yan AM, Nguyen-Dang H. Multiple-cracked fatigue crack growth by BEM. Comput Mech 1995;16:273–280.

[7] Fish J, Markolefas S, Guttal R, Nayak P. On adaptive multilevel superposition of finite element meshes for linear elastostatics. Appl Numer Math 1994;14:135–164.

[8] Kikuchi M, Wada Y, Shintaku Y. Fatigue crack growth simulation in heterogeneous material using s-version FEM. Int J Fatigue 2014;58:47–55.

[9] Melenk J, Babuska I. The partition of unity finite element method: basic theory and applications. Comput Methods Appl Mech Eng 1996;139:289–314.

[10] Moes N, Dolbow J, Belytschko T. A finite element method for crack growth without remeshing. Int J Numer Methods Eng 1999;46:131–150.

[11] Sukumar N, Moes N, Moran B, Belytschko T. Extended finite element method for three-dimensional crack modelling. Int J Numer Methods Eng 2000;48:1549–1570.

[12] Moes N, Gravouil A, Belytschko T. Non-planar 3D crack growth by the extended finite element and level sets-Part I:Mechanical model. Int J Numer Methods Eng 2002;53:2549–2568.

[13] Sukumar N, Prevost J-H. Modeling quasi-static crack growth with the extended finite element method Part I: Computer implementation. Int J Solids Struct 2003;40:7513-7537.

[14] Singh IV, Mishra BK, Bhattacharya, Patil RU. The numerical simulation of fatigue crack growth using extended finite element method. Int J Fract 2012;36:109-119.

[15] Pathak H, Singh A, Indra VS. Fatigue crack growth simulations of 3-D problems using XFEM. Int J Mech Sci 2013;76:112-131.

[16] Kumar S, Singh IV, Mishra BK, Rabczuk T. Modeling and simulation of kinked cracks by virtual node XFEM. Comput Methods Appl Mech Engrg 2015;283:1425–1466.

[17] Wu SC, Zhang SQ, Xu ZW. Thermal crack growth-based fatigue life prediction due to braking for a high-speed railway brake disc. Int J Fract 2016;87:359-369.

[18] Tang XH, Wu SC, Zheng C, Zhang JH. A novel virtual node method for polygonal elements. Appl Math Mech 2009;30(10):1233–1246.

[19] Wu SC, Peng X, Zhang WH, Stephane SPA. The virtual node polygonal element method for nonlinear thermal analysis with application to hybrid laser welding. Int J Heat Mass Transf 2013;67(3):1247–1254.

[20] Tian R, Wen LF. Improved XFEM—An extra-dof free, well-conditioning, and interpolating XFEM. Comput Methods Appl Mech Engrg 2015;285:639–658.

[21] Ma S, Zhang XB, Recho N, Li J. The mixed-mode investigation of the fatigue crack in CTS metallic specimen. Int J Fract 2006;28:1780-1790.